BioMACROMOLECULES

pubs.acs.org/Biomac

Article

Protein Desorption Kinetics Depends on the Timescale of Observation

Kaixuan Lyu, Hongbo Chen, Jing Gao, Jing Jin, Hengchong Shi, Daniel K. Schwartz,* and Dapeng Wang*

Cite This: https://doi.org/10.1021/acs.biomac.2c00917

Read Online

ABSTRACT: The presence of so-called reversible and irreversible protein adsorption on solid surfaces is well documented in the literature and represents the basis for the development of nanoparticles and implant materials to control interactions in physiological environments. Here, using a series of complementary single-molecule tracking approaches appropriate for different timescales, we show that protein desorption kinetics is much more complex than the traditional reversible−irreversible binary picture. Instead, we find that the surface residence time distribution of adsorbed proteins transitions from power law to exponential behavior when measured over a large range of timescales (10^{-2}−10^{6} s). A comparison with macroscopic results obtained using a quartz crystal microbalance suggested that macroscopic measurements have generally failed to observe such nonequilibrium phenomena because they are obscured by ensemble-averaging effects. These findings provide new insights into the complex phenomena associated with protein adsorption and desorption.

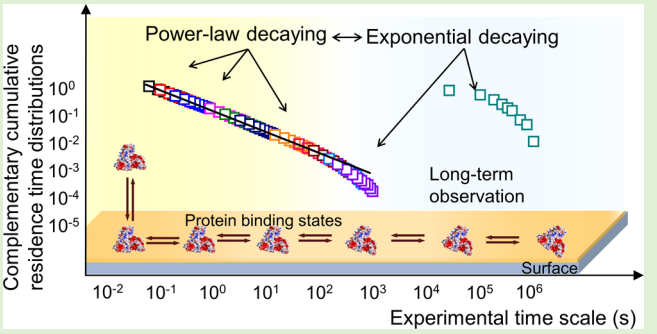

INTRODUCTION

Protein adsorption occurs rapidly when a solid surface comes into contact with protein-containing biological fluids.[1−3] It is generally accepted that cellular responses to materials in a biological medium reflect the composition of adsorbed protein layer rather than the material itself.[4−9] In particular, the adsorbed protein layer modulates biological/cellular responses to implanted healthcare materials and the pathophysiology/toxicity of nanoparticles for drug/gene delivery systems.[10−14] Therefore, it is important to understand and characterize how proteins adsorb to and desorb from surfaces, which is often characterized by exposing a surface to protein solution and measuring the net accumulation over time until an apparent adsorption−desorption equilibrium is reached.[15] Such experimental observations can be fitted to theoretical models, such as a Langmuir adsorption isotherm or derivative models, to yield kinetic parameters associated with adsorption and desorption.[2] This fitting approach is widely practiced but may lead to incorrect mechanistic conclusions.[16,17] For example, it is frequently observed in adsorption experiments that when a surface is first incubated with a protein solution, and then subsequently exposed to a solution that does not contain protein, a population of "irreversibly" adsorbed protein molecules remains on the surface for timescales much longer than the accessible measurement time.[18−20] Interestingly, the presence of "irreversibly" adsorbed species can paradoxically appear to be consistent with an apparent Langmuir isotherm.[21] This scenario highlights the fact that an apparent agreement between a model and experimental data does not necessarily justify the underlying hypothesis of the model. In such a case, fitting the theoretical model to an experimental protein adsorption isotherm serves only to produce erroneous values of the equilibrium constant or kinetic parameters such as the adsorption and desorption rate constants k_a and k_d.[22]

To address this concern, a bottom-up approach using single-molecule tracking methods was proposed because it enables the direct, model-free quantification of distinct microscopic processes such as adsorption, surface diffusion, and desorption of fluorescently labeled molecules at liquid−liquid and solid−liquid interfaces under steady-state conditions.[23−28] However, kinetic parameters acquired in such experiments, such as the adsorption and desorption rate constants k_a and k_d, are sensitive to the characteristic timescales of the experiments. For example, the k_d of bovine serum albumin (BSA) on a fused silica surface is measured to be approximately 0.3 s^{-1} when using single-molecule tracking with an image acquisition time t_{ac} = 0.1 s. Comparatively, an early single-molecule study with

Received: July 26, 2022
Revised: September 15, 2022

Table 1. Structural and Property Parameters of Two Model Proteins

protein	M_W[a]	isoelectric point	size[b]	PDB ID[c]
BSA	66.7 kD	4.9	215.7 × 45.1 × 142.4 Å^3	3V03
transferrin	79 kD	5.5	45.0 × 57.9 × 135.9 Å^3	1D4N

[a]M_W = Molecule weight. [b]Size = The unit cell parameters of protein crystal structures. [c]PDB ID = Protein Data Bank identification.

relatively low temporal resolution analyzed total BSA coverage as a function of time with a Langmuir model and found k_d = 0.02 s^{-1}.[29,30] An important question arising from this apparent inconsistency is whether the timescale on which desorption is observed influences the apparent characteristic residence time that will be obtained. Moreover, it is important to understand how these microscopic observations can be reconciled with macroscopic ensemble-averaging measurements.

Here, we designed single-molecule tracking experiments to study the desorption kinetics of two representative plasma proteins, bovine serum albumin (BSA) and transferrin, at solid−liquid interfaces on characteristic timescales ranging from 10^{-2} to 10^{6} s using a series of complementary measurements involving single-molecule tracking with systematically varied temporal resolution. We found that the measured characteristic residence time τ of the adsorbed proteins was observation-time-dependent and that this was consistent with surface-mediated aging effects where a small but important population of adsorbed protein molecules converted from weakly to strongly adsorbed states. Interestingly, protein residence time distributions exhibited a power-law decay for times shorter than 400 s and exponential decay for longer timescales. A comparison with results from a common analytical technique suggested that the complex aging and nonequilibrium effects associated with protein surface residence are often masked by ensemble averaging in traditional macroscopic measurements.

EXPERIMENTAL METHODS

Protein Solutions. Phosphate-buffered saline (PBS) with pH = 7.2−7.4 was used to prepare all protein solutions. The proteins used in this study, BSA and transferrin were purchased from Aladdin Chemistry Co., Ltd., China, and OKA, China, respectively, and labeled with fluorescent dyes. The structural and property parameters of two plasma proteins are shown in Table 1[31,32] Labeling was performed using ATTO 647 (ATTO−TEC, Germany) and CF640 (Biotium), which are amine-reactive reagents with *N*-hydroxysuccinimidyl-terminated groups. The fluorescent labeling was performed using protocols described by the manufacturers. The fluorescently labeled proteins were purified from residual free fluorescent dyes using multiple passes through desalting columns (GE Healthcare). All protein sample solutions were purified at least two times to remove free fluorophore molecules. Using a UV−vis spectrometer, we determined that one dye was attached per protein molecule on average. Fluorescence correlation spectroscopy measurements indicated that free dye molecules were not detected in the dye-labeled BSA and transferrin solutions (Figure S1).

Surface Preparation. Borosilicate glass wafers (Deckgläser, Germany) were immersed in 80 °C piranha solution for 3 h, followed by thorough rinsing with Milli-Q water (18.2 MΩ·cm) and dried using a nitrogen stream. For amine-functionalized surfaces, wafers were placed in a vacuum desiccator with a solution containing 1 mL of toluene, 500 μL of (3-aminopropyl)triethoxysilane (Aladdin, China), and 100 μL of *N*,*N*-diisopropylethylamine (Aladdin, China) for 48 h at room temperature. Trimethylsilane (TMS) surfaces were prepared by exposing wafers to hexamethyldisilazane (Alfa Aesar, China) vapor for 48 h. Following silanization, wafers were rinsed with ethanol and Milli-Q water and dried under nitrogen gas before use. The static water contact angles of the amine-functionalized surfaces and TMS surfaces were 42 and 90°, respectively, consistent with previous observations.[33]

To accurately quantify the desorption of individual protein molecules from a solid−liquid interface, dye-labeled proteins were diluted to a concentration of 10^{-12} M in PBS. Protein solutions were filtered to remove possible aggregates. The protein solution was added into an Attofluor chamber that was then sealed to eliminate the water evaporation; the protein concentration is expected to remain constant throughout the experiment.

Single-Molecule Tracking. Single-molecule localization measurements were performed using a Ti2-E total internal reflection fluorescence microscope (TIRFM) in conjunction with a high numerical aperture 100× oil immersion objective. The measurements were performed at 22 °C. An EMCCD camera (iXon DU897) operating at −70 °C was employed to capture sequences of images. ATTO 647 labeled BSA and CF640 labeled transferrin were excited using a continuous-wave 640 nm OBIS-LX diode laser. TIRFM exploits the evanescent field upon total reflection of an incident laser at a solid−liquid interface to selectively excite fluorescent molecules within a layer of ∼100 nm of the solid−liquid interface on the aqueous side. Because of the fast diffusion coefficient of labeled proteins in the solution (Figure S1), proteins in the solution were not resolved. Each TIRFM measurement requires calibration for the stage drift. This was resolved using a feedback control system with fiducial markers, permitting hour- or even day-long observation.

We applied three distinct approaches to acquire surface residence time distributions in different timescale regimes. First, in a direct acquisition scheme, we varied the image acquisition time t_{ac} over which the EMCCD camera counted photons to produce a single fluorescence image (Figure 1C). The image acquisition times used were t_{ac} = 0.03, 0.05, 0.1, 0.5, 1, and 2 s; more than 50 movies with 800 frames each were taken at each value t_{ac}. The positions of labeled protein molecules were identified in each image and molecular trajectories were extracted from the image sequences using a custom-developed tracking algorithm as described previously. For each t_{ac}, at least 10^4 objects with a duration of longer than 2 frames were extracted and analyzed. Second, in a time-lapse acquisition scheme, the time interval t_{ti} between consecutive image acquisitions was the relevant timescale, as shown in Figure 1D. In these measurements, we chose t_{ac} = 0.1 s and t_{ti} = 0.5, 1, 10, 30, 60, 120, and 180 s, respectively. A high-speed optical shutter was synchronized with the camera acquisition. More than 50 movies with 50 frames each were taken at each value of t_{ti}. Third, in a long timescale direct desorption scheme, a solid surface was initially exposed to protein solution at a concentration of 10^{-12} M (10^{-7} mg/mL) for 1 h. The protein solution was then replaced with pure PBS (not containing protein), allowing the direct measurement of desorption from the surface by counting the mean number of adsorbed protein molecules per unit area every 24 h until the adsorbed protein molecules were removed. The total exposure time over 15 days was 1.5 s. Control experiments indicated that the disappearance of protein molecules from the surface was not caused by photobleaching.

Quartz Crystal Microbalance (QCM). A QCM measurement system (Q-Sense E4, Sweden) was equipped with a flow cell (QFM401, Sweden) to create a flow chamber in which the temperature was controlled. A multichannel peristaltic pump (IPC Ismatec SA, Switzerland) was used to flow the aqueous solution through the flow cell over a 14 mm diameter 5 MHz crystal. QCM crystals with Cr/Au electrodes (RQ5MTAP, China) were cleaned before use using piranha solution and rinsing with deionized water. Amine-functionalized surfaces were prepared by depositing self-assembled monolayers (SAMs) of 3-amino-1-propanethiol (Alfa,

https://doi.org/10.1021/acs.biomac.2c00917
Biomacromolecules XXXX, XXX, XXX−XXX

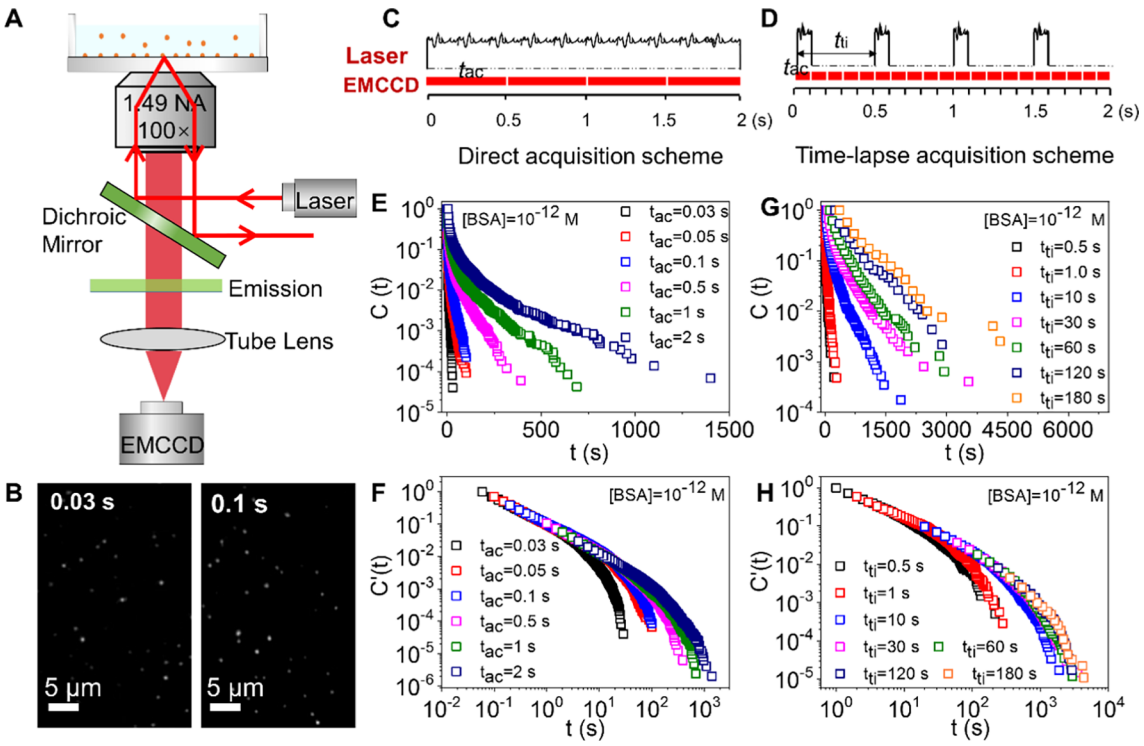

Figure 1. Dependence of desorption kinetics on timescales of observation. (A) Schematic representation of TIRFM. (B) Representative fluorescence images acquired at t_{ac} = 0.03 and 0.1 s, respectively. Schematic diagrams of (C) direct and (D) time-lapse acquisition schemes. (E) CCRTDs and (F) their normalization obtained by direct acquisition with various t_{ac} for BSA at solid−liquid interfaces. (G) CCRTDs and (H) their normalization obtained by time-lapse acquisition with various t_{ti}.

China). The QCM crystals were incubated in 1 mM ethanolic solution of the thiol for at least 12 h, rinsed with ethanol, and dried under nitrogen before use. Protein solutions with given concentrations were injected at a constant flow rate of 50 μL min^{-1}, and the resonance frequency of the crystal oscillator was monitored continuously. The oscillation of the crystal was modified by protein adsorption to the crystal surface, shifting the resonant frequency because of a change in total coupled mass. The Sauerbrey equation was used to relate the measured frequency shift (Δf) and the adsorbed mass per unit area (M) as follows

$$M = -C\frac{\Delta f}{n} \quad (1)$$

where n is the frequency overtone number (1, 3, ···) and C is the mass sensitivity constant with a value of 17.7 ng cm^{-2} Hz^{-1} at 5 MHz.

RESULTS AND DISCUSSION

Single-Molecule Tracking at Different Timescales. We employed TIRFM to identify the adsorption and desorption of individual fluorescently labeled BSA and transferrin at the interface between aqueous solution and amine-functionalized solid surfaces (Figure 1A). For a given TIRFM measurement, one must choose a specific temporal setting with which to observe the system. For TIRFM with continuous illumination, the relevant timescale is the image acquisition time (t_{ac}) over which the EMCCD camera counts photons for an individual fluorescence image (Figure 1C). To maximize temporal resolution, the shortest t_{ac} with a sufficient signal-to-noise ratio to ensure proper object identification is frequently chosen. However, noise, blinking, photobleaching, and inevitable "broken trajectories" upon tracking with an automated algorithm can cause artificial loss of objects.[34,35] Increasing t_{ac} decreases the temporal resolution but also decreases object loss from tracking artifacts. Thus, while the decreased temporal resolution associated with longer t_{ac} values permits the observation of strong, long-lived adsorbents, it cannot identify the residence of adsorbents much shorter than t_{ac}. Therefore, combining complementary information from various t_{ac} values can widen the observable time range of the residence time, as described in previous work.[34]

Figure 1B shows representative images for adsorbed BSA at solid−liquid interfaces with two different values of t_{ac}. Fluorophores can be localized with an adequate signal-to-background ratio at the shortest t_{ac} = 0.03 s. Adsorbed BSA molecules were immobile; diffusion was not observed on amine-functionalized surfaces (Figure S2), consistent with previous work studying similar systems.[33,36] Immobilization was important in this study because it permitted the long-time tracking of individual molecules. Figures 1E and S4 show the complementary cumulative residence time distributions (CCRTDs) of BSA at various t_{ac}. The CCRTD was calculated to represent the fraction of molecules that remain on the surface for time t or longer after adsorption. Data from an exponential distribution for a single mean characteristic residence time would appear as a straight line on the semilogarithmic axes of Figure 1E. This is clearly not the case for any t_{ac} studied; however, the CCRTDs can be fit by an exponential mixture model with three populations to yield the weighted average of residence time τ (Supporting Information). We used the CCRTD obtained at t_{ac} = 0.03 s as a reference; each subsequent CCRTD was multiplied by a factor to shift downward to match its value at the smallest (leftmost) t-axis value with the relevant value of the CCRTD obtained using a shorter t_{ac}. In this way, the CCRTDs obtained at various t_{ac} can superimpose complementarily over extended

https://doi.org/10.1021/acs.biomac.2c00917
Biomacromolecules XXXX, XXX, XXX−XXX

timescales.[34] As shown in Figure 1F, a clear (approximately power law) decay was observed as a downward deviation for residence times longer than ~100t_{ac}. The acquired CCRTDs are robust and do not depend on the excitation intensity when it is higher than a threshold value (Figure S3), indicating that the downward deviation was not caused by photobleaching (An enhanced downward deviation would be present for high excitation intensity where more serious photobleaching might occur). Previous work pointed out a nonzero probability of losing objects could be responsible for the downward deviation.[34] Interestingly, the emergence of an apparent power-law form of CCRTDs at short timescales is consistent with previous work studying the desorption kinetics of plasma proteins at interfaces between aqueous solution and hydrophobic, hydrophilic, and nonfouling surfaces.[33,37−39]

Because the fluorescent dyes would eventually photobleach under continuous laser illumination, a time-lapse scheme was employed to provide information about longer residence times. In particular, images were obtained at time intervals separated by t_{ti}, ignoring events that occurred during the intervening intervals (laser-off time) (Figure 1D). In a representative measurement, a 50-frame time-lapse movie was obtained, in which the objects that appeared in the first and last frames were ignored (because their true residence times could not be determined). The upper limit for laser illumination was therefore 50t_{ac} = 5 s. The characteristic timescale of fluorophore photobleaching was quantified by covalently attaching protein molecules on the solid surface and measuring the rate of object loss.[40] The obtained mean photobleaching time of 170 ± 10 s was much longer than laser exposure time, suggesting that photobleaching did not play a substantial role. The CCRTDs obtained using the time-lapse scheme with various t_{ti} are presented in Figure 1G. For $t_{ti} \leq 30$ s, the CCRTDs decay as a power-law function and can only be approximated by an exponential mixture model (SI). Interestingly, we found that the time-lapse CCRTDs decayed exponentially with residence time (linearly on a log-linear scale) when $t_{ti} > 30$ s (Figures 1G and S6), with an apparent time constant that depended on the time-lapse interval. This apparent exponential decay was confirmed by implementing a nonparametric Kolmogorov−Smirnov (KS) test to directly evaluate the raw data points and circumvent model-dependent interpretation.[41] Therefore, we found that the time-lapse CCRTD decay exhibited an apparent power law to exponential crossover as t_{ti} increased from 0.5 to 180 s. Interestingly, data acquired at different t_{ti} values can be superimposed into a master distribution with a downward deviation emerging only in the long residence time range (Figure 1H). This indicated that the use of data obtained at various t_{ac} or t_{ti} can extend the timescale of individual measurements when using different acquisition schemes with a series of t_{ac} or t_{ti} values.

We note that each acquisition scheme has its advantages. The direct acquisition scheme offers direct observation over time but suffers from the finite length of observation time due to photobleaching. Moreover, the signal-to-background ratio decreases with decreasing t_{ac}, increasing the probability of losing objects. On the other hand, the time-lapse acquisition enables longer observation but suffers from the loss of information between image acquisition events. It is important to ask whether the use of these two schemes with $t_{ac} = t_{ti}$ yields consistent results and whether bias was introduced into the acquired data by varying t_{ac} or t_{ti}. We analyzed the results and determined that consistent results were obtained using the two different schemes with $t_{ac} = t_{ti}$; representative results are shown in Figure 2A. The comparison indicated that results were

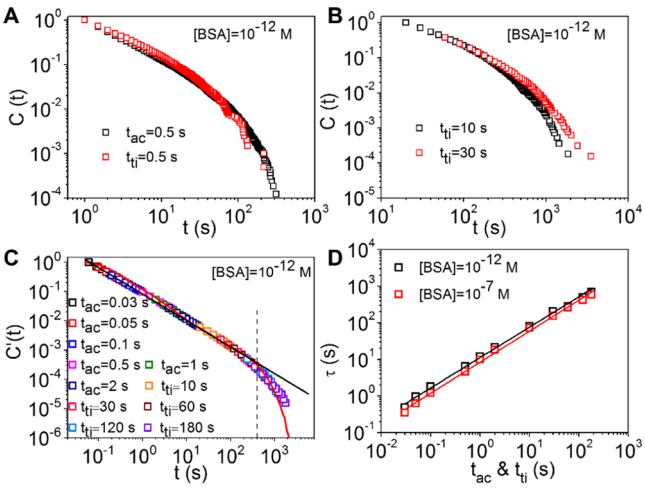

Figure 2. Residence time distribution exhibiting a power law to exponential transition. (A) CCRTDs obtained using direct and time-lapse acquisition schemes with $t_{ac} = t_{ti} = 0.5$ s. (B) CCRTDs obtained using the time-lapse acquisition scheme with t_{ti} = 10 and 30 s. (C) Normalization of truncated CCRTDs obtained using both schemes with all t_{ac} and t_{ti} values studied; the red solid line represents a fit using a state-balance model. (D) Mean characteristic surface residence times of BSA on amine-functionalized surfaces obtained using different schemes with varying t_{ac} and t_{ti} at bulk concentrations of 10^{-7} and 10^{-12} M.

consistent, albeit with different total laser exposure times. Further, we compared the CCRTD data acquired at two representative t_{ti} values of 10 and 30 s (Figure 2B); the data overlapped perfectly in the range of small-to-moderate residence times but inevitably deviated at longer residence times. To account for these artifacts, in each measurement, we counted only measured residence times that were less than 10 t_{ac} or 10 t_{ti}, and used the same normalization method as shown in Figure 1F to combine all data obtained using different acquisition schemes into a single master curve, as shown in Figure 2C. Considering this master curve, for residence times t < 400 s, $C'(t) \propto t^{-0.9}$ for more than four orders of magnitude in time. For t > 400 s, $C'(t)$ can be well approximated by an exponential function as verified by a KS test with a characteristic residence time of 435 s.

The data described above were obtained at an ultra-low fractional surface coverage by area (10^{-6}). To further test the robustness and universality of the aforementioned finding, we studied desorption kinetics at a higher bulk BSA concentration (10^{-7} M) where the equilibrium fractional surface coverage was approximately 10^{-1}. We found that the power law to exponential crossover was preserved at the higher coverage (Figure S7), with a modest but systematic decrease in the characteristic residence times (τ) acquired at different timescales (Figure 2D), presumably due to the preferential blocking of anomalously strong adsorption sites.[33] Further, we studied other factors such as surface chemistry and the use of different plasma proteins to verify that the heterogeneous protein desorption observed here (i.e., the crossover from power law to the exponential decay of CCRTD) was a general phenomenon, and not specific to a given type of protein on a given surface. The desorption of BSA from a TMS surface and

https://doi.org/10.1021/acs.biomac.2c00917
Biomacromolecules XXXX, XXX, XXX−XXX

transferrin from amine-functionalized surfaces were measured at t_{ac} = 0.1 s and t_{ti} = 180 s, respectively. In these two sets of experiments, the CCRTDs obtained at t_{ac} = 0.1 s followed a power-law decay, while CCRTDs obtained at t_{ti} = 180 s were well described by a single exponential decay (Figure S8). These results illustrate that the power law to exponential crossover is a universal phenomenon spanning diverse concentrations, surfaces, and proteins.

Long-Term Measurements to Quantify "Irreversibly" Adsorbed Objects. When we performed measurements using the time-lapse scheme with the longest t_{ti} = 180 s, we found that a small fraction of BSA molecules remained adsorbed to the surface over the entire time course of the experiment, signifying that the observations were truncated at longer timescales. Even aggressive rinsing failed to remove these molecules from the surface. An obvious question emerged as to whether the adsorption of these objects was truly irreversible or whether this fraction simply has a characteristic timescale for desorption that is much longer than the experimental observations. We attempted to address this question by first exposing a surface to proteins in solution, subsequently replacing the protein solution with protein-free PBS, and monitoring the net number of adsorbed proteins over time. One limitation of this approach is that following desorption from the surface, protein molecules can experience multiple unproductive surface encounters and finally readsorb on the surface.[42] Indeed, over long observation times, the net number of adsorbed proteins may remain erroneously constant over time because of this effect (Figure S9). To address this, we designed a microfluidic chamber that enabled single-molecule measurement under laminar flow (Figure 3A), which would

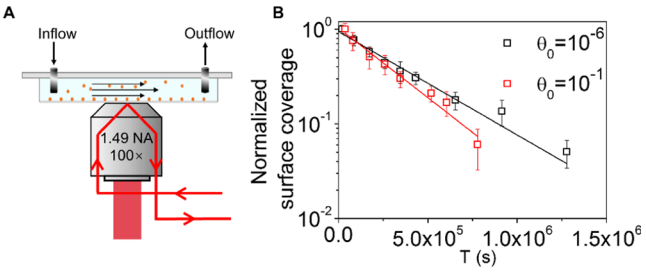

Figure 3. Long-term desorption kinetics. (A) Schematic representation of a microfluidic chamber integrated with the TIRF microscope. (B) Normalized surface coverage as a function of the measurement time for different initial concentrations. θ_0 is the initial fractional surface coverage by area.

tend to remove a desorbed molecule from the field of view. In these experiments, BSA solution at a concentration of 10^{-12} M flowed for 1 h. The solution was then exchanged to protein-free PBS at a flow rate of 1 μL min^{-1} for 5 h to remove adsorbed BSA molecules with residence times shorter than 5 h. The number of adsorbed proteins decreased rapidly with time because the desorbed proteins were removed with the buffer flow (Figure S10). A small population of proteins remained adsorbed at the solid–liquid interface after 5 h rinsing. To provide results with statistical significance, more than 10^3 molecules were subsequently acquired from more than 50 images at multiple locations. Then, a fluorescence image was manually obtained at 24 h intervals over a total period of 15 days until the surface coverage is close to zero.

Figure 3B shows the surface coverage of proteins evolved with time when the flow rate was 1 μL min^{-1}. Varying the flow rate in the range of 1–100 μL min^{-1} did not change the results. The surface coverage decreased monotonically with time and finally approached zero, suggesting that the apparently irreversible adsorption resulted from adsorbed protein molecules with characteristic desorption times far beyond the typical time course of an experiment. Over a sufficiently long timescale, the desorption kinetics can be adequately described by a single exponential decay with timescales T_{long} = 3.98 × 10^5 and 2.96 × 10^5 s for surface coverages of 10^{-6} and 10^{-1}, respectively. Thus, consistent with the observations at shorter timescales, increasing the surface coverage caused shorter residence of proteins at solid–liquid interfaces (Figure 3B).

Combined with the results in previous sections, these observations indicated that desorption occurs at timescales from 10^{-2} to 10^6 s. The extrapolation of the CCRTDs to short times indicated an increased number of desorption or collision events for times shorter than 10^{-2} s.[43] However, due to the limited temporal resolution, protein molecules colliding with the surface and diffusing back into the solution at such short timescales were treated only as background noise. The fact that CCRTDs exhibited a shape that was much broader than a single exponential at short times suggested the existence of a spectrum of binding energies. This can originate from either a nonstationary process[44,45] where the binding energy varied with time or a heterogeneous process[46] involving multiple binding energies that can be approximated by a superposition of exponential functions. Previous studies found that apparent power-law CCRTDs can often be adequately described as the sum of contributions from multiple, independent, and simultaneously occurring exponential processes because of the formation of a range of protein aggregates.[39,47] Moreover, protein molecules can potentially interact with a given interface in different ways (e.g., different conformations or orientations[17]), leading to a broad distribution of adsorption states corresponding to different binding energies.[22,48−50] The complex desorption process can be modeled as an initially adsorbed object that performs random walk over a rugged energy landscape.[37]

Protein Desorption Exhibits Aging. To understand the most likely underlying mechanism leading to the broad range of timescales, we designed a specific set of analyses and measurements. First, we carefully checked and ruled out the effect of protein aggregation on desorption kinetics. Specifically, the protein solutions were filtered to remove any aggregates before use. Moreover, fluorescence correlation spectroscopy measurements indicated no aggregation in the solution even when the solution was left standing for 30 days (SI). We also considered the possibility that surface-induced aggregation may occur, especially in long-term experiments. However, we calculated that the collision probability of two proteins meeting at the interface was only 0.01% under the conditions of the experiments, suggesting a negligible chance of surface-induced aggregation. Because even trace amounts of protein aggregates are hypothesized to enrich at the solid–liquid interface because of their higher interfacial affinity than the protein monomer, we explicitly checked for the presence of such aggregates by looking for signatures involving brighter fluorescence emission and longer surface residence times than a monomer.[39] However, when we measured the fluorescence intensity distributions using a time-lapse scheme with various

https://doi.org/10.1021/acs.biomac.2c00917
Biomacromolecules XXXX, XXX, XXX−XXX

t_{ti} (Figure 4A), the distributions of fluorescence intensities were analogous for all values of t_{ti}; only one distinct peak was

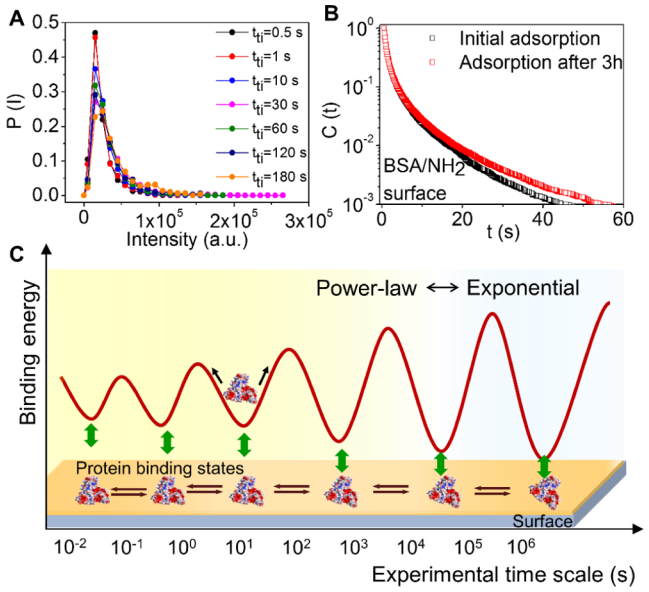

Figure 4. Protein desorption exhibiting aging. (A) Fluorescence intensity distributions of adsorbed BSA measured at different t_{ti}. (B) Complementary cumulative residence time distributions of BSA on amine-functionalized surfaces measured immediately after sample preparation or after 3 h. (C) Schematic illustration for surface protein aging originated from the reversible conversion of various binding states with distinct binding energies.

observed at the same intensity value for all temporal settings. Also, when the acquisition time was fixed at t_{ac} = 0.1 s, we found that the fluorescence intensity was not correlated with the residence time (Figure S11). Taken together, all of these facts and observations strongly suggested that protein aggregation was not responsible for the observation-time-dependent desorption kinetics.

We further considered the possibility that protein desorption was a nonstationary process that evolved with time. To this end, we used the direct acquisition scheme with t_{ac} = 0.1 s to comparatively study desorption kinetics under two conditions: immediately after sample preparation vs after allowing the sample to relax for 3 h prior to measurements (Figure 4B). Interestingly, we found that the CCRTDs tail at longer timescales decayed systematically more slowly after 3 h relaxation. This suggested that after 3 h relaxation, the majority of BSA molecules contacting the surface exhibited short-lived residence times, and desorbed without any conformational or orientational change. However, a minority of BSA molecules became kinetically trapped, denoting an aging effect. To selectively study the population with long-time relaxation, we imaged multiple areas of the surface and specifically focused on the trajectories that appeared in the first frame of movies. We found that the CCRTDs associated with these trajectories after 3 h relaxation decayed more slowly than the freshly prepared ones (Figure S12).

We speculate that the observed aging can be attributed to surface-mediated relaxation, indeed this is consistent with previous findings suggesting that the structure of adsorbed proteins often becomes increasingly denatured over time.[51,52] Therefore, we hypothesized that surface protein aging was caused by the reversible conversion of multiple binding states corresponding to different values of τ. To test this hypothesis quantitatively, we modeled CCRTDs using kinetic Monte Carlo simulations involving a state-balance model.[37] The simulation details are described in the SI. In short, the desorption energy exploration can be modeled as a biased random walk on a rugged one-dimensional energy landscape possessing a number (N) of wells of various depths, each of which corresponds to specific binding energy (Figure 4C). A BSA molecule initially adsorbs at a solid−liquid interface in the state with the shallowest well. The BSA molecules can either desorb rapidly from the surface with probability p or into a state with a deeper well with probability $1 - p$. At sufficiently long times, a fraction of protein molecules can fall into the deepest well. These simulations employed experimentally measured characteristic times at six observation timescales as inputs; the only adjustable parameter was p. Note that $p = 0.5$ indicates an equal chance of conversion to weaker and stronger states and $p > 0.5$ denotes a bias toward weaker binding states. By setting $p = 0.83$, the simulations successfully represented the experimental CCRTDs obtained by accumulating data from multiple observation timescales (Figure 2C). Taken together, the consistent systematic trends seen in both simulations and experimental results suggest that the interconversion between distinct states with a bias toward weaker binding states leads to CCRTDs that exhibit a power law to exponential crossover.

Comparison to Results Obtained by QCM. It is interesting to compare the above direct observations of protein desorption kinetics over eight orders of magnitude with results obtained using a traditional ensemble technique.[53] To this end, we compared single-molecule data with the results obtained using QCM under nominally identical experimental conditions. QCM is one of the most prevalent ensemble-averaging techniques for the characterization of surface adsorption by measuring changes in the resonant frequency of a crystal oscillator.[54] QCM exhibits distinct advantages over many other traditional methods because it allows an in situ, time-dependent measure of the adsorbed mass on the oscillator surface. Figure 5A exhibits representative time courses of the

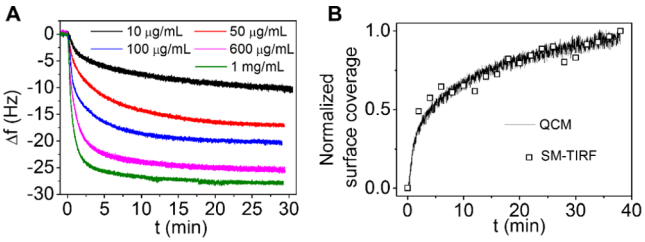

Figure 5. Comparison between results obtained by single-molecule tracking and QCM. (A) Frequency shifts vs exposure time for BSA adsorption on amine-functionalized surfaces. (B) Normalized surface coverage vs time of BSA on amine-functionalized surfaces measured by QCM and SM-TIRF, respectively.

frequency shift of the crystal oscillator upon the addition of fluorescently labeled BSA at various concentrations. The frequency shift (Δf) is defined as the difference between the actual resonance frequency $f(t)$ and the initial frequency $f(t = 0)$. The apparent surface coverage of BSA can be calculated from Δf using eq 1. In QCM measurements, the adsorption and desorption rate constants were determined using a Langmuir model; we obtained $k_a = 2.77 \times 10^3$ (mol L^{-1})$^{-1}$

https://doi.org/10.1021/acs.biomac.2c00917
Biomacromolecules XXXX, XXX, XXX−XXX

s^{-1} and k_d = 2.24 × 10^{-3} s^{-1}, which were similar to results obtained by QCM under similar conditions[30,55] (the details are described in the SI). Interestingly, we found that the measured k_d agreed quantitatively with the results of single-molecule measurements using the time-lapse acquisition scheme with t_{ti} = 120 and 180 s (Figure 2D).

Furthermore, to make a quantitative comparison, we measured the total surface coverage of adsorbed BSA, $\theta(t)$, at a solid−liquid interface as a function of time t under nominally identical conditions using both types of technique. Remarkable consistency in $\theta(t)$ was observed (Figure 5B). Interestingly, the analysis of TIRFM movies indicated that short-lived objects were in rapid exchange with the bulk solution and represented a large fraction of the full ensemble and that long-lived objects represented only a small contribution toward the surface coverage.

From an experimental point of view, each type of measurement was biased to recognize one or several adsorbed states in a given range of timescales. One might argue that the only populations of importance are those that dominate the surface coverage. However, the observation in Figure 4B indicates that the conversion from a short-lived to a long-lived population is a critical feature of protein adsorption which cannot be properly understood without the acknowledgment of the short-lived state. Moreover, it is well known that a protein layer can form rapidly (less than a few seconds) on a nanoparticle surface when in contact with a biological medium.[3] A temporal evolution from a loosely attached to an irreversible attached protein on nanoparticles was also observed.[56−58] Considering only an ensemble-average observation, it would be tempting to conclude that direct protein—surface attraction increased with time on such a surface when, in fact, the underlying mechanism, involving an aging effect, is completely different. While proteins are in rapid exchange between solution and surface, a small fraction of adsorbed proteins converts to a more stable adsorbed state. As time involves, more and more short-lived proteins convert into their long-lived counterparts, resulting in the time evolution of a protein layer.

CONCLUSIONS

Here we performed a mixed scheme of single-molecule tracking experiments to follow the desorption kinetics of representative plasma proteins, BSA, and transferrin at solid−liquid interfaces over a wide range of timescales, 10^{-2}−10^{6} s, by combining information obtained at different temporal settings. We found that the characteristic residence time of adsorbed proteins was observation-time-dependent where longer observation times led to an increase in the apparent characteristic residence time, arising from the exploration of a desorption energy landscape over time, i.e., exhibiting aging. On timescales from 10^{-2} to 10^{4} s, the residence time distribution exhibited a power law to exponential transition. Tracking desorption from the solid−liquid interface on timescales of 10^{4}−10^{6} s yielded an exponentially distributed residence time. The residence time distribution can be quantitatively described by a state-balance model involving sequential and reversible jumps to explore a rugged energy landscape possessing wells with a broad distribution of binding energy depths. Comparison with results obtained using QCM shows excellent consistency, indicating that the focus on a time-dependent average surface coverage neglected complexities that were masked by ensemble averaging. While protein adsorption and desorption are often characterized by exposing a surface to protein solution and measuring the net accumulation over time to yield k_a and k_d, this approach is potentially insensitive to short-lived proteins because they do not contribute to the calculation of k_a and k_d. However, such proteins may be relevant and important for technological and biomedical applications. As we demonstrate here, it is important to reevaluate protein adsorption and the biological identity of material surfaces by measuring the surface residence over multiple orders of magnitude in time. These results reveal limitations of traditional methods that are generally biased toward desorption events in a narrow range of timescales. More nuanced measurements should account for the observable time window attempting to understand complex protein adsorption and desorption phenomena. We hope that the complementary single-molecule tracking approaches can serve as a benchmark for the characterization of protein desorption kinetics and that subsequent studies will use this approach to characterize the desorption kinetics of additional proteins.

ASSOCIATED CONTENT

Supporting Information

The Supporting Information is available free of charge at https://pubs.acs.org/doi/10.1021/acs.biomac.2c00917.

Fluorescence correlation spectroscopy (FCS); time-averaged mean squared displacement (TA-MSD); complementary cumulative residence time distributions (CCRTD); effects of excitation intensity and the universality of protein heterogeneous desorption behavior; details of a transition of CCRTDs from power law to exponential decay with increasing interval time; and Monte Carlo simulation for binding states of protein to surfaces (PDF)

AUTHOR INFORMATION

Corresponding Authors

Daniel K. Schwartz − *Department of Chemical and Biological Engineering, University of Colorado Boulder, Boulder, Colorado 80309, United States;* orcid.org/0000-0001-5397-7200; Email: daniel.schwartz@colorado.edu

Dapeng Wang − *State Key Laboratory of Polymer Physics and Chemistry, Changchun Institute of Applied Chemistry, Chinese Academy of Sciences, Changchun 130022, P. R. China; University of Science and Technology of China, Hefei 230026, P. R. China;* orcid.org/0000-0003-0276-7152; Email: wdp@ciac.ac.cn

Authors

Kaixuan Lyu − *State Key Laboratory of Polymer Physics and Chemistry, Changchun Institute of Applied Chemistry, Chinese Academy of Sciences, Changchun 130022, P. R. China; University of Science and Technology of China, Hefei 230026, P. R. China;* orcid.org/0000-0001-8935-8751

Hongbo Chen − *State Key Laboratory of Polymer Physics and Chemistry, Changchun Institute of Applied Chemistry, Chinese Academy of Sciences, Changchun 130022, P. R. China*

Jing Gao − *State Key Laboratory of Electroanalytical Chemistry, Changchun Institute of Applied Chemistry, Chinese Academy of Sciences, Changchun 130022, P. R. China*

https://doi.org/10.1021/acs.biomac.2c00917
Biomacromolecules XXXX, XXX, XXX−XXX

Jing Jin − *State Key Laboratory of Polymer Physics and Chemistry, Changchun Institute of Applied Chemistry, Chinese Academy of Sciences, Changchun 130022, P. R. China;* orcid.org/0000-0002-2710-4243

Hengchong Shi − *State Key Laboratory of Polymer Physics and Chemistry, Changchun Institute of Applied Chemistry, Chinese Academy of Sciences, Changchun 130022, P. R. China;* orcid.org/0000-0002-7549-0388

Complete contact information is available at: https://pubs.acs.org/10.1021/acs.biomac.2c00917

Author Contributions

K.L. and H.C. contributed equally.

Notes

The authors declare no competing financial interest.

■ ACKNOWLEDGMENTS

Financial support from the National Natural Science Foundation of China (nos. 22073091 and 21873094), National Key Research and Development Program of China (nos. 2021YFC2101700 and 2021YFF0306400), International Science and Technology Cooperation Program of Jilin, China (nos. 20220508126RC), and Key Research Program of Frontier Sciences, Chinese Academy of Sciences (no. ZDBS-LY-SLH033) are gratefully acknowledged.

■ REFERENCES

(1) Wei, Q.; Becherer, T.; Angioletti-Uberti, S.; Dzubiella, J.; Wischke, C.; Neffe, A. T.; Lendlein, A.; Ballauff, M.; Haag, R. Protein Interactions with Polymer Coatings and Biomaterials. *Angew. Chem., Int. Ed.* **2014**, *53*, 8004−8031.

(2) Rabe, M.; Verdes, D.; Seeger, S. Understanding Protein Adsorption Phenomena at Solid Surfaces. *Adv. Colloid Interface Sci.* **2011**, *162*, 87−106.

(3) Morsbach, S.; Gonella, G.; Mailander, V.; Wegner, S.; Wu, S.; Weidner, T.; Berger, R.; Koynov, K.; Vollmer, D.; Encinas, N.; Kuan, S. L.; Bereau, T.; Kremer, K.; Weil, T.; Bonn, M.; Butt, H. J.; Landfester, K. Engineering Proteins at Interfaces: From Complementary Characterization to Material Surfaces with Designed Functions. *Angew. Chem., Int. Ed.* **2018**, *57*, 12626−12648.

(4) Walczyk, D.; Bombelli, F. B.; Monopoli, M. P.; Lynch, I.; Dawson, K. A. What the Cell "Sees" in Bionanoscience. *J. Am. Chem. Soc.* **2010**, *132*, 5761−5768.

(5) Weiss, A. C. G.; Kempe, K.; Forster, S.; Caruso, F. Microfluidic Examination of the "Hard" Biomolecular Corona Formed on Engineered Particles in Different Biological Milieu. *Biomacromolecules* **2018**, *19*, 2580−2594.

(6) Walkey, C. D.; Chan, W. C. Understanding and Controlling the Interaction of Nanomaterials with Proteins in a Physiological Environment. *Chem. Soc. Rev.* **2012**, *41*, 2780−2799.

(7) Park, J. H.; Jackman, J. A.; Ferhan, A. R.; Belling, J. N.; Mokrzecka, N.; Weiss, P. S.; Cho, N. J. Cloaking Silica Nanoparticles with Functional Protein Coatings for Reduced Complement Activation and Cellular Uptake. *ACS Nano* **2020**, *14*, 11950−11961.

(8) Wang, H.; Shang, L.; Maffre, P.; Hohmann, S.; Kirschhofer, F.; Brenner-Weiss, G.; Nienhaus, G. U. The Nature of a Hard Protein Corona Forming on Quantum Dots Exposed to Human Blood Serum. *Small* **2016**, *12*, 5836−5844.

(9) Monopoli, M. P.; Aberg, C.; Salvati, A.; Dawson, K. A. Biomolecular Coronas Provide the Biological Identity of Nanosized Materials. *Nat. Nanotechnol.* **2012**, *7*, 779−786.

(10) Wang, L.; Li, J.; Pan, J.; Jiang, X.; Ji, Y.; Li, Y.; Qu, Y.; Zhao, Y.; Wu, X.; Chen, C. Revealing the Binding Structure of the Protein Corona on Gold Nanorods Using Synchrotron Radiation-Based Techniques: Understanding the Reduced Damage in Cell Membranes. *J. Am. Chem. Soc.* **2013**, *135*, 17359−17368.

(11) Schöttler, S.; Becker, G.; Winzen, S.; Steinbach, T.; Mohr, K.; Landfester, K.; Mailander, V.; Wurm, F. R. Protein Adsorption Is Required for Stealth Effect of Poly(ethylene glycol)-and Poly-(phosphoester)-Coated Nanocarriers. *Nat. Nanotechnol.* **2016**, *11*, 372−377.

(12) Weiss, A. C. G.; Kelly, H. G.; Faria, M.; Besford, Q. A.; Wheatley, A. K.; Ang, C. S.; Crampin, E. J.; Caruso, F.; Kent, S. J. Link between Low-Fouling and Stealth: A Whole Blood Biomolecular Corona and Cellular Association Analysis on Nanoengineered Particles. *ACS Nano* **2019**, *13*, 4980−4991.

(13) Tenzer, S.; Docter, D.; Kuharev, J.; Musyanovych, A.; Fetz, V.; Hecht, R.; Schlenk, F.; Fischer, D.; Kiouptsi, K.; Reinhardt, C.; Landfester, K.; Schild, H.; Maskos, M.; Knauer, S. K.; Stauber, R. H. Rapid Formation of Plasma Protein Corona Critically Affects Nanoparticle Pathophysiology. *Nat. Nanotechnol.* **2013**, *8*, 772−781.

(14) Firkowska-Boden, I.; Zhang, X.; Jandt, K. D. Controlling Protein Adsorption through Nanostructured Polymeric Surfaces. *Adv. Healthcare Mater.* **2018**, *7*, No. 1700995.

(15) Chen, S.; Zheng, J.; Li, L.; Jiang, S. Strong Resistance of Phosphorylcholine Self-Assembled Monolayers to Protein Adsorption: Insights into Nonfouling Properties of Zwitterionic Materials. *J. Am. Chem. Soc.* **2005**, *127*, 14473−14478.

(16) Latour, R. A. The Langmuir Isotherm: A Commonly Applied but Misleading Approach for the Analysis of Protein Adsorption Behavior. *J. Biomed. Mater. Res., Part A* **2015**, *103*, 949−958.

(17) Kastantin, M.; Langdon, B. B.; Schwartz, D. K. A Bottom-Up Approach to Understanding Protein Layer Formation at Solid-Liquid Interfaces. *Adv. Colloid Interface Sci.* **2014**, *207*, 240−252.

(18) Hadjidemetriou, M.; Kostarelos, K. Nanomedicine Evolution of the Nanoparticle Corona. *Nat. Nanotechnol.* **2017**, *12*, 288−290.

(19) Milani, S.; Bombelli, F. B.; Pitek, A. S.; Dawson, K. A.; Radler, J. Reversible versus Irreversible Binding of Transferrin to Polystyrene Nanoparticles: Soft and Hard Corona. *ACS Nano* **2012**, *6*, 2532−2541.

(20) Höök, F.; Rodahl, M.; Kasemo, B.; Brzezinski, P. Structural Changes in Hemoglobin during Adsorption to Solid Surfaces: Effects of pH, Ionic Strength, and Ligand Binding. *Proc. Natl. Acad. Sci. U.S.A.* **1998**, *95*, 12271−12276.

(21) Adamczyk, Z. Protein Adsorption: A Quest for a Universal Mechanism. *Curr. Opin. Colloid Interface Sci.* **2019**, *41*, 50−65.

(22) Latour, R. A. Fundamental Principles of the Thermodynamics and Kinetics of Protein Adsorption to Material Surfaces. *Colloids Surf., B* **2020**, *191*, No. 110992.

(23) Wang, D.; Hu, R.; Skaug, M. J.; Schwartz, D. K. Temporally Anticorrelated Motion of Nanoparticles at a Liquid Interface. *J. Phys. Chem. Lett.* **2015**, *6*, 54−59.

(24) Wang, D.; Zhu, Y. L.; Zhao, Y.; Li, C. Y.; Mukhopadhyay, A.; Sun, Z. Y.; Koynov, K.; Butt, H. J. Brownian Diffusion of Individual Janus Nanoparticles at Water/Oil Interfaces. *ACS Nano* **2020**, *14*, 10095−10103.

(25) Dominguez-Medina, S.; Kisley, L.; Tauzin, L. J.; Hoggard, A.; Shuang, B.; Indrasekara, A. S.; Chen, S.; Wang, L. Y.; Derry, P. J.; Liopo, A.; Zubarev, E. R.; Landes, C. F.; Link, S. Adsorption and Unfolding of a Single Protein Triggers Nanoparticle Aggregation. *ACS Nano* **2016**, *10*, 2103−2112.

(26) Kisley, L.; Chen, J.; Mansur, A. P.; Shuang, B.; Kourentzi, K.; Poongavanam, M. V.; Chen, W. H.; Dhamane, S.; Willson, R. C.; Landes, C. F. Unified Superresolution Experiments and Stochastic Theory Provide Mechanistic Insight into Protein Ion-Exchange Adsorptive Separations. *Proc. Natl. Acad. Sci. U.S.A.* **2014**, *111*, 2075−2080.

(27) Niu, Q.; Wang, D. Probing the Polymer Anomalous Dynamics at Solid/Liquid Interfaces at the Single-Molecule Level. *Curr. Opin. Colloid Interface Sci.* **2019**, *39*, 162−172.

(28) Zhao, Y.; Lu, Y.; Wang, D. Tracking of Nanoparticle Diffusion at a Liquid-Liquid Interface Adsorbed by Nonionic Surfactants. *Langmuir* **2021**, *37*, 12118−12127.

(29) Yeung, K. M.; Lu, Z. J.; Cheung, N. H. Adsorption of Bovine Serum Albumin on Fused Silica: Elucidation of Protein-Protein

Interactions by Single-Molecule Fluorescence Microscopy. *Colloids Surf., B* **2009**, *69*, 246−250.
(30) Kwok, K. C.; Yeung, K. M.; Cheung, N. H. Adsorption Kinetics of Bovine Serum Albumin on Fused Silica: Population Heterogeneities Revealed by Single-Molecule Fluorescence Microscopy. *Langmuir* **2007**, *23*, 1948−1952.
(31) Majorek, K. A.; Porebski, P. J.; Dayal, A.; Zimmerman, M. D.; Jablonska, K.; Stewart, A. J.; Chruszcz, M.; Minor, W. Structural and Immunologic Characterization of Bovine, Horse, and Rabbit Serum Albumins. *Mol. Immunol.* **2012**, *52*, 174−182.
(32) Yang, A. H. W.; Macgillivray, R. T. A.; Chen, J.; Luo, Y.; Wang, Y.; Brayer, G. D.; Mason, A. B.; Woodworth, R. C.; Murphy, M. E. P. Crystal Structures of Two Mutants (K206Q, H207E) of the N-Lobe of Human Transferrin with Increased Affinity for Iron. *Protein Sci.* **2008**, *9*, 49−52.
(33) Cai, Y.; Schwartz, D. K. Influence of Protein Surface Coverage on Anomalously Strong Adsorption Sites. *ACS Appl. Mater. Interfaces* **2016**, *8*, 511−520.
(34) Kastantin, M.; Schwartz, D. K. Identifying Multiple Populations from Single-Molecule Lifetime Distributions. *ChemPhysChem* **2013**, *14*, 374−380.
(35) Shen, H.; Tauzin, L. J.; Baiyasi, R.; Wang, W.; Moringo, N.; Shuang, B.; Landes, C. F. Single Particle Tracking: From Theory to Biophysical Applications. *Chem. Rev.* **2017**, *117*, 7331−7376.
(36) Krapf, D.; Campagnola, G.; Nepal, K.; Peersen, O. B. Strange Kinetics of Bulk-Mediated Diffusion on Lipid Bilayers. *Phys. Chem. Chem. Phys.* **2016**, *18*, 12633−12641.
(37) Armstrong, M. J.; Rodriguez, J. B., III; Dahl, P.; Salamon, P.; Hess, H.; Katira, P. Power Law Behavior in Protein Desorption Kinetics Originating from Sequential Binding and Unbinding. *Langmuir* **2020**, *36*, 13527−13534.
(38) Shen, H.; Tauzin, L. J.; Wang, W.; Hoener, B.; Shuang, B.; Kisley, L.; Hoggard, A.; Landes, C. F. Single-Molecule Kinetics of Protein Adsorption on Thin Nylon-6,6 Films. *Anal. Chem.* **2016**, *88*, 9926−9933.
(39) Hedayati, M.; Kipper, M. J.; Krapf, D. Anomalous Protein Kinetics on Low-Fouling Surfaces. *Phys. Chem. Chem. Phys.* **2020**, *22*, 5264−5271.
(40) McLoughlin, S. Y.; Kastantin, M.; Schwartz, D. K.; Kaar, J. L. Single-Molecule Resolution of Protein Structure and Interfacial Dynamics on Biomaterial Surfaces. *Proc. Natl. Acad. Sci. U.S.A.* **2013**, *110*, 19396−19401.
(41) Massey, F. J. The Kolmogorov-Smirnov Test for Goodness of Fit. *J. Am. Stat. Assoc.* **1951**, *46*, 68−78.
(42) Wang, D.; Wu, H.; Schwartz, D. K. Three-Dimensional Tracking of Interfacial Hopping Diffusion. *Phys. Rev. Lett.* **2017**, *119*, No. 268001.
(43) Wang, W.; Shen, H.; Moringo, N. A.; Carrejo, N. C.; Ye, F.; Robinson, J. T.; Landes, C. F. Super-Temporal-Resolved Microscopy Reveals Multistep Desorption Kinetics of α-Lactalbumin from Nylon. *Langmuir* **2018**, *34*, 6697−6702.
(44) Hu, X.; Hong, L.; Dean Smith, M.; Neusius, T.; Cheng, X.; Smith, J. C. The Dynamics of Single Protein Molecules Is Non-Equilibrium and Self-Similar over Thirteen Decades in Time. *Nat. Phys.* **2016**, *12*, 171−174.
(45) Zhang, S.; Sadre, R.; Legg, B. A.; Pyles, H.; Perciano, T.; Bethel, E. W.; Baker, D.; Rubel, O.; De Yoreo, J. J. Rotational Dynamics and Transition Mechanisms of Surface-Adsorbed Proteins. *Proc. Natl. Acad. Sci. U.S.A.* **2022**, *119*, No. e2020242119.
(46) Burov, S.; Jeon, J. H.; Metzler, R.; Barkai, E. Single Particle Tracking in Systems Showing Anomalous Diffusion: The Role of Weak Ergodicity Breaking. *Phys. Chem. Chem. Phys.* **2011**, *13*, 1800−1812.
(47) Kastantin, M.; Langdon, B. B.; Chang, E. L.; Schwartz, D. K. Single-Molecule Resolution of Interfacial Fibrinogen Behavior: Effects of Oligomer Populations and Surface Chemistry. *J. Am. Chem. Soc.* **2011**, *133*, 4975−4983.
(48) Penna, M. J.; Mijajlovic, M.; Biggs, M. J. Molecular-Level Understanding of Protein Adsorption at the Interface between Water and a Strongly Interacting Uncharged Solid Surface. *J. Am. Chem. Soc.* **2014**, *136*, 5323−5331.
(49) Fleischer, C. C.; Payne, C. K. Secondary Structure of Corona Proteins Determines the Cell Surface Receptors Used by Nanoparticles. *J. Phys. Chem. B* **2014**, *118*, 14017−14026.
(50) Peng, B.; Yang, Z.; Yang, L.; Chen, J.; Liu, L.; Wang, D. Reducing the Solvent Quality Gives Rise to the Outward Migration of a Star Polymer in Poiseuille Flow. *Macromolecules* **2022**, *55*, 3396−3407.
(51) Roach, P.; Farrar, D.; Perry, C. C. Interpretation of Protein Adsorption: Surface-Induced Conformational Changes. *J. Am. Chem. Soc.* **2005**, *127*, 8168−8173.
(52) Calonder, C.; Tie, Y.; Van Tassel, P. R. History Dependence of Protein Adsorption Kinetics. *Proc. Natl. Acad. Sci. U.S.A.* **2001**, *98*, 10664−10669.
(53) Hedayati, M.; Marruecos, D. F.; Krapf, D.; Kaar, J. L.; Kipper, M. J. Protein Adsorption Measurements on Low Fouling and Ultralow Fouling Surfaces: A Critical Comparison of Surface Characterization Techniques. *Acta Biomater.* **2020**, *102*, 169−180.
(54) Carrillo-Carrion, C.; Carril, M.; Parak, W. J. Techniques for the Experimental Investigation of the Protein Corona. *Curr. Opin. Biotechnol.* **2017**, *46*, 106−113.
(55) Goda, T.; Maeda, Y.; Miyahara, Y. Simultaneous Monitoring of Protein Adsorption Kinetics Using a Quartz Crystal Microbalance and Field-Effect Transistor Integrated Device. *Anal. Chem.* **2012**, *84*, 7308−7314.
(56) Casals, E.; Pfaller, T.; Duschl, A.; Oostingh, G. J.; Puntes, V. Time Evolution of the Nanoparticle Protein Corona. *ACS Nano* **2010**, *4*, 3623−3632.
(57) Weiss, A. C. G.; Kruger, K.; Besford, Q. A.; Schlenk, M.; Kempe, K.; Forster, S.; Caruso, F. In Situ Characterization of Protein Corona Formation on Silica Microparticles Using Confocal Laser Scanning Microscopy Combined with Microfluidics. *ACS Appl. Mater. Interfaces* **2019**, *11*, 2459−2469.
(58) Latreille, P. L.; Le Goas, M.; Salimi, S.; Robert, J.; De Crescenzo, G.; Boffito, D. C.; Martinez, V. A.; Hildgen, P.; Banquy, X. Scratching the Surface of the Protein Corona: Challenging Measurements and Controversies. *ACS Nano* **2022**, *16*, 1689−1707.

https://doi.org/10.1021/acs.biomac.2c00917
Biomacromolecules XXXX, XXX, XXX−XXX